Inorganic Chemistry

Article

pubs.acs.org/IC

Tuning Spin−Spin Coupling in Quinonoid-Bridged Dicopper(II) Complexes through Rational Bridge Variation

David Schweinfurth,[†] Marat M. Khusniyarov,*[,‡] Denis Bubrin,[§] Stephan Hohloch,[†] Cheng-Yong Su,[∥] and Biprajit Sarkar*[,†]

[†]Institut für Chemie und Biochemie, Freie Universität Berlin, Fabeckstrasse 34-36, D-14195, Berlin, Germany

[‡]Department Chemie und Pharmazie, Friedrich-Alexander-Universität Erlangen-Nürnberg, Egerlandstrasse 1, 91058, Erlangen, Germany

[§]Institut für Anorganische Chemie, Universität Stuttgart, Pfaffenwaldring 55, D-70569, Stuttgart, Germany

[∥]Lehn Institute of Functional Materials, School of Chemistry and Chemical Engineering, Sun Yat-Sen University, Guangzhou, 510275, China

Supporting Information

ABSTRACT: Bridged metal complexes $[\{Cu(tmpa)\}_2(\mu\text{-}L^1_{-2H})](ClO_4)_2$ (**1**), $[\{Cu(tmpa)\}_2(\mu\text{-}L^2_{-2H})](ClO_4)_2$ (**2**), $[\{Cu(tmpa)\}_2(\mu\text{-}L^3_{-2H})](BPh_4)_2$ (**3**), and $[\{Cu(tmpa)\}_2(\mu\text{-}L^4_{-2H})](ClO_4)_2$ (**4**) (tmpa = tris(2-pyridylmethyl)amine, L^1 = chloranilic acid, L^2 = 2,5-dihydroxy-1,4-benzoquinone, L^3 = (2,5-di-[2-(methoxy)-anilino]-1,4-benzoquinone, L^4 = azophenine) were synthesized from copper(II) salts, tmpa, and the bridging quinonoid ligands in the presence of a base. X-ray structural characterization of the complexes showed a distorted octahedral environment around the copper(II) centers for the complexes **1**−**3**, the donors being the nitrogen atoms of tmpa, and the nitrogen or oxygen donors of the bridging quinones. In contrast, the copper(II) centers in **4** display a distorted square-pyramidal coordination, where one of the pyridine arms of each tmpa remains uncoordinated. Bond-length analyses within the bridging ligand exhibit localization of the double bonds inside the bridge for **1**−**3**. In contrast, complete delocalization of double bonds within the bridging ligand is observed for **4**. Temperature-dependent magnetic susceptibility measurements on the complexes reveal an antiferromagnetic coupling between the copper(II) ions. The strength of antiferromagnetic coupling was observed to depend on the energy of the HOMO of the bridging quinone ligands, with exchange coupling constants J in the range between −23.2 and −0.6 cm^{-1} and the strength of antiferromagnetic coupling of **4** > **3** > **2** > **1**. Broken-symmetry density functional theory calculations (DFT) revealed that the orientation of magnetic orbitals in **1** and **2** is different than that in **3** and **4**, and this results in two different exchange pathways. These results demonstrate how bridge-mediated spin−spin coupling in quinone-bridged metal complexes can be strongly tuned by a rational design of the bridging ligand employing the [O] for [NR] isoelectronic analogy.

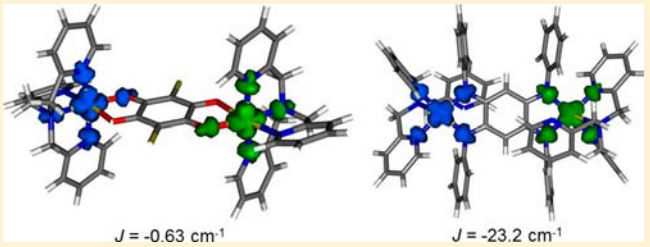

INTRODUCTION

Bridge-mediated spin−spin coupling has been an extremely important phenomenon in magnetochemistry, and, more recently, in molecular magnetism.[1] In that regard, the bridging ligand chloranilic acid (CA) in its doubly deprotonated form has been used for investigating spin−spin coupling in dicopper(II) complexes, as well as in copper(II) coordination polymers.[2,3] In a seminal work,[4] Kahn and co-workers pointed out the various factors that can be used for influencing spin−spin coupling between two copper(II) centers bridged by an organic ligand. One of the important factors influencing such spin−spin coupling in dicopper(II) complexes is the energy level of the bridge-based highest occupied molecular orbital (HOMO), and the other one is the coordination geometry around the copper(II) centers. In that seminal work, Kahn and co-workers addressed this issue by substituting the "C−Cl" chlorides of the CA bridge by various halides and the NO_2 group (Scheme 1).[4]

Scheme 1. Variations in the Bridging Ligand Used by Kahn *et al.*[4] To Investigate the Effect of Bridge Substitution on the Strength of Spin−Spin Coupling

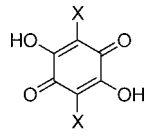

X = Cl, Br, I, NO_2

The hope was to be able to influence the energy level of the bridge-based HOMO by changing the electronegativity of the substituents on the CA bridge. The influence of such a substitution on the spin−spin coupling turned out to be marginal

Received: April 17, 2013
Published: September 6, 2013

Scheme 2. Bridge Variation Used in This Work by Using the [O] for [NR] Isoelectronic Analogy

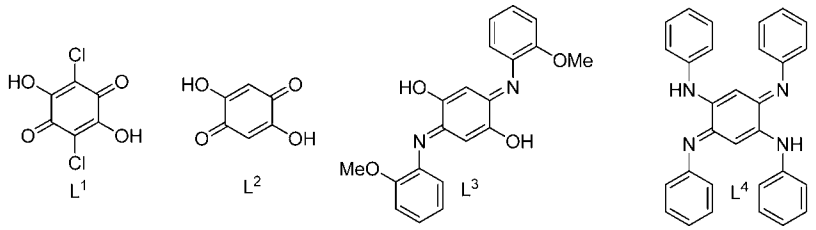

Table 1. Crystallographic Details

	1	2	3	4
formula	$C_{46}H_{52}Cl_4Cu_2N_8O_{16}$	$C_{44}H_{46}Cl_2Cu_2N_8O_{14}$	$C_{109}H_{102}B_2Cu_2N_{10}O_{5.5}$	$C_{66}H_{58}Cl_2Cu_2N_{12}O_8$
M_r	1241.84	1108.87	1788.71	1345.22
crystal system	triclinic	monoclinic	triclinic	monoclinic
space group	$P\bar{1}$	$P2_1/c$	$P\bar{1}$	$P2_1/c$
a (Å)	10.898(2)	9.403(2)	11.572(5)	11.1420(1)
b (Å)	11.903(2)	14.796(3)	17.606(5)	19.6064(2)
c (Å)	12.648(3)	17.155(4)	23.800(5)	14.7665(2)
α (deg)	114.92(1)	90	97.797(5)	90
β (deg)	111.09(1)	90.11(1)	100.695(5)	111.539(1)
γ (deg)	94.63(1)	90	92.277(5)	90
V (Å^3)	1334.9(4)	2386.7(9)	4710(3)	3000.54(6)
Z	1	2	2	2
D_{calc} (g cm^{-3})	1.545	1.543	1.261	1.489
T (K)	173(2)	173(2)	150(2)	150(2)
radiation source	Mo Kα	Mo Kα	Mo Kα	Cu Kα
μ (mm^{-1})	1.072	1.078	0.512	2.260
F(000)	638	1140	1876	1388
meas./indep. refl.	5224/4952	4982/4689	29 997/14807	17 299/4744
obsvd. [$I > 2\sigma(I)$] refl.	4325	3719	12 615	4393
R(int)	0.0479	0.0263	0.0366	0.0224
$R[F^2 > 2\sigma(F^2)]$	0.0372	0.0335	0.0585	0.0347
wR (F^2)	0.1104	0.0942	0.1912	0.0973
S	1.121	0.981	1.023	1.048
$\Delta\rho_{max}$, $\Delta\rho_{min}$ (e Å^{-3})	0.518, −0.479	0.556, −0.363	1.282, −0.802	0.640, −0.724

despite the HOMO level of the bridge being influenced by such a substitution pattern. It was rightly pointed out that the weak influence of the bridge substitution on the strength of spin−spin coupling in dicopper(II) complexes was related to the fact that the substituted halides in CA bear only marginal spin density.[4] We argued that, if changes in the bridge are to influence spin−spin coupling in a significant way, the best way to do this would be to substitute the donor atoms that directly coordinate to the paramagnetic metal centers. This is because the coordinating donor atoms are likely to get substantial spin density via delocalization of spin density through a formation of covalent metal−ligand bond.

In recent years, our group and others have been active in the synthesis of new types of bridging quinone ligands by using the [O] for [NR] isoelectronic analogy in the popularly used bridging ligand 1,4-dihydroxy-2,5-benzoquinone (dhbq).[5] Thus, various ligands shown in Scheme 2[6] have been reported by us and others, and these ligands and their metal complexes have been used for investigating electron transfer properties and mixed-valency,[7] magnetic properties,[8] homogeneous catalysis,[9] and in supramolecular chemistry.[10] Additionally, azophenine (L^4) is a potentially bridging ligand that has only nitrogen donor sets.[11] Even though some reports on metal complexes of azophenine and related ligands have appeared in recent years,[12] the coordination chemistry of this potentially bridging quinone ligand has remained largely neglected.

We were thus interested in investigating the following issue: What would be the effect on spin−spin coupling in dicopper(II) complexes if the donor set in the bridging quinone ligand is varied from [O,O,O,O] through [O,N,O,N] to [N,N,N,N]? As a coligand, we chose a potentially tetradentate tripodal ligand tmpa (tmpa = tris(2-pyridylmethyl)amine) that has been recently used successfully for synthesizing metal complexes for performing biomimetic studies, and for investigating electron transfer processes.[7e,13] In the following, we present details on the synthesis, single-crystal X-ray diffraction, and magnetic properties of the complexes $[\{Cu(tmpa)\}_2(\mu\text{-}L^1{}_{-2H})](ClO_4)_2$ (**1**), $[\{Cu(tmpa)\}_2(\mu\text{-}L^2{}_{-2H})](ClO_4)_2$ (**2**), $[\{Cu(tmpa)\}_2(\mu\text{-}L^3{}_{-2H})](BPh_4)_2$ (**3**), and $[\{Cu(tmpa)\}_2(\mu\text{-}L^4{}_{-2H})](ClO_4)_2$ (**4**) (L^1 = chloranilic acid, L^2 = 2,5-dihydroxy-1,4-benzoquinone, L^3 = (2,5-di-[2-(methoxy)-anilino]-1,4-benzoquinone, L^4 = azophenine) to answer the above formulated questions. In addition, we also describe results from DFT calculations on these complexes to address the question of the amount of spin density on the coordinating atoms of the bridge.

RESULTS AND DISCUSSION

Synthesis and Crystal Structures. The complexes **1**−**4** were synthesized by the in situ generation of a "Cu(tmpa)"

dx.doi.org/10.1021/ic400955c | Inorg. Chem. 2013, 52, 10332−10339

precursor, and the subsequent addition of the deprotonated forms of the respective ligands (see the Experimental Section). Whereas **1**−**3** were obtained in good yields, the yield of **4** was low. The deprotonation of L^4 and its subsequent metalation turned out to be trickier than those for the other ligands. Unidentified side-products were formed during this reaction, which led to the relatively low yields of **4**. All complexes passed combustion tests, and an excellent match was obtained between the calculated and the experimental C, H, and N values.

Single crystals could be obtained for all the complexes, and these were subjected to X-ray diffraction studies. Complexes **1** and **3** crystallized in the triclinic $P\bar{1}$ space group, whereas **2** and **4** crystallized in the monoclinic $P2_1/c$ space group (Table 1).

In complexes **1**−**3**, the copper(II) centers are in a distorted octahedral environment (Figures 1−3). The distortion from an

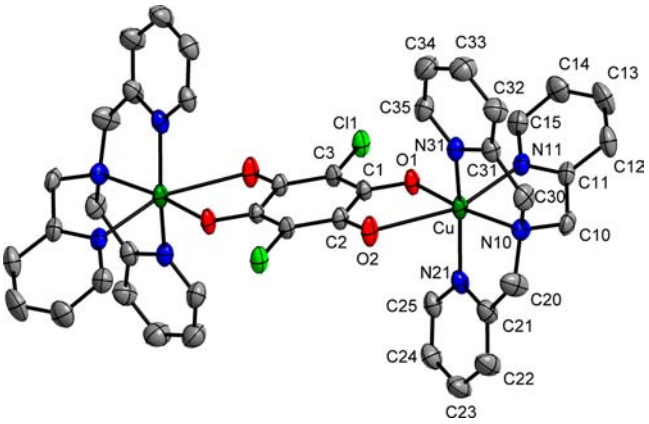

Figure 1. ORTEP plot of **1**. Ellipsoids are drawn at 50% probability. Hydrogen atoms and counteranions have been omitted for clarity.

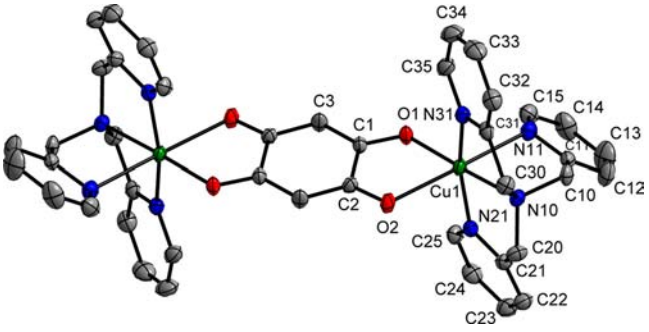

Figure 2. ORTEP plot of **2**. Ellipsoids are drawn at 50% probability. Hydrogen atoms and counteranions have been omitted for clarity.

ideal octahedral environment is caused by the chelating nature of tmpa and the bridging quinone ligands and also due to a Jahn−Teller effect for d^9 copper(II) centers.[1a]

The copper−ligand bond distances show some interesting differences between the complexes **1**−**3**. For complexes **1** and **2**, the longest axis around the copper center (O2−Cu1−N11) is the one containing the Cu−O2 and the Cu−N11 bonds. All other distances between the copper centers and the donor atoms are shorter than the distances mentioned above (Table 2). Thus, the elongated axis (due to Jahn−Teller distortion) of the octahedron is the one that contains a donor atom of the bridging ligand. Some consequences of this are a relatively short Cu1−N10(amine) distance of 2.057(2) Å for both **1** and **2**, despite an amine nitrogen not being a very good donor. The other effect

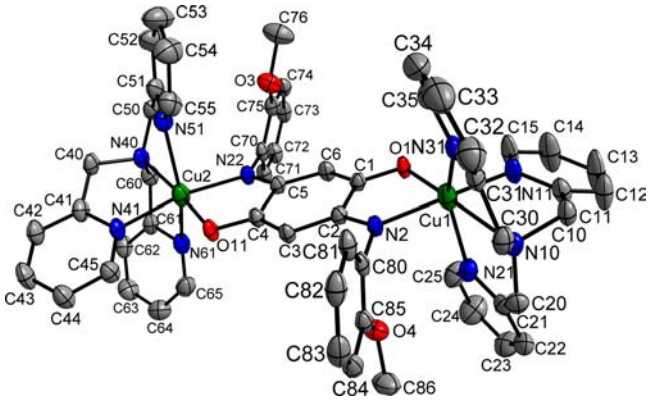

Figure 3. ORTEP plot of **3**. Ellipsoids are drawn at 50% probability. Hydrogen atoms and counteranions have been omitted for clarity.

Table 2. Selected Metal−Ligand Bond Lengths in Angstroms in Complexes 1−4 Derived from Single-Crystal X-ray Diffraction Studies

	1	2	3	4
Cu1−O1/Cu1−N1	1.954(2)	1.965(2)	2.024(2)	1.979(2)
Cu1−O2/Cu1−N2	2.550(3)	2.309(2)	1.985(3)	1.971(2)
Cu1−N10	2.057(2)	2.057(2)	2.278(3)	2.370(2)
Cu1−N11	2.257(2)	2.389(2)	2.012(3)	2.054(2)
Cu1−N21	2.012(2)	2.020(2)	2.305(3)	1.997(2)
Cu1−N31	2.023(2)	2.005(2)	2.256(3)	3.781(3)
Cu2−O11			1.944(2)	
Cu2−N22			2.018(3)	
Cu2−N40			2.132(3)	
Cu2−N41			2.014(3)	
Cu2−N51			2.306(3)	
Cu2−N61			2.562(3)	

is the large difference between the Cu1−O1 and the Cu1−O2 distances (1.954(2) and 2.550(3) Å for **1**). Such large differences between copper(II) and the two "O" donors of the ligand L^1 have been observed for related copper(II) complexes before.[3] These data point to the fact that the magnetic orbital $d_{x_2-y_2}$ of the copper(II) center is oriented along the O1−Cu−N10 and the N21−Cu−N31 axes for the complexes **1** and **2** and is not in the plane of the bridging ligand. (*The axis containing the longest metal−ligand bond is taken as the Jahn−Teller axis throughout the text, and the d_{z_2} orbital is fixed along that axis.*)[3]

In contrast to **1** and **2**, the longest axes of the octahedron around the copper(II) centers for **3** are N21−Cu1−N31 and N51−Cu2−N61 (Table 2). The donor atoms along these axes are the pyridine nitrogen atoms of tmpa. Thus, for **3**, the elongated axis is perpendicular to the plane of the bridging ligand. For **3**, the magnetic orbitals $d_{x_2-y_2}$ of the copper(II) centers are thus oriented in the plane of the bridging ligand.[3]

Analysis of the bond lengths inside the bridging ligands shows that, for **1** and **2**, the C1−O1 bonds are longer than the C2−O2 bonds. Accordingly, the C1−C3 bonds are shorter than the C2−C3 bonds (Table 3). The C1−C2 bond at about 1.5 Å for both **1** and **2** is longer than the other C−C bonds and is in the range of a C−C single bond. Thus, the double bonds in the bridging ligands in **1** and **2** are localized and the bridging ligands bind to the copper(II) centers through two neutral keto-type oxygen donors (C═O) and two anionic alkoxy-type donors ($C-O^-$) (Scheme

dx.doi.org/10.1021/ic400955c | *Inorg. Chem.* 2013, 52, 10332−10339

Table 3. Selected Intraligand Bond Lengths in Angstroms in Complexes 1−4 Derived from Single-Crystal X-ray Diffraction Studies

	1	2	3	4
C1−O1/C1−N1	1.279(3)	1.282(3)	1.285(4)	1.327(3)
C2−O2/C2−N2	1.239(3)	1.254(3)	1.302(4)	1.327(3)
C4−O11			1.295(4)	
C5−N22			1.312(4)	
C1−C2	1.538(3)	1.547(3)	1.505(4)	1.499(3)
C1−C3/C1−C6	1.377(3)	1.389(3)	1.376(4)	1.392(3)
C2−C3	1.426(3)	1.410(3)	1.418(4)	1.395(3)
C3−C4			1.363(4)	
C4−C5			1.506(4)	
C5−C6			1.415(4)	

3). Such a bridging mode is thus best described as a bis(alkoxy)-*p*-quinone type of coordination.

Scheme 3. Schematic Representation of the Coordinated Bridging Ligands Showing the Localizations of Double Bonds in 1−3 and Delocalization in 4

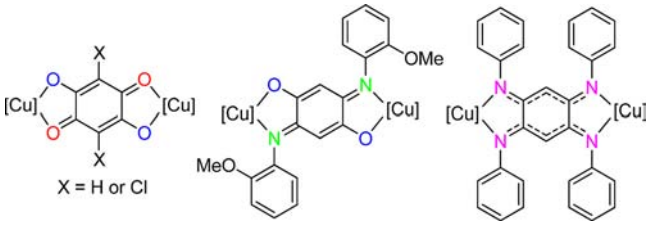

Similar to **1** and **2**, the double bonds inside the bridging ligands in **3** are localized as well (Table 3), with the donor atoms taking the form of anionic alkoxy "C−O$^-$" and neutral imino "C═N" type of donors. The coordination mode of the bridging ligand L^3_{-2H} is thus best described as bis(imino)-bis(alkoxy) type (Scheme 3). Similar types of coordination modes for ligands related to L^3_{-2H} have been observed by us recently for dinuclear complexes with other metal centers.[7e−g] The 2-methoxy-phenyl substituents on the bridging ligand in **3** are perpendicular to the plane containing the donor atoms of the bridging ligand.

In contrast to **1**−**3** that display a distorted octahedral coordination around the copper(II) centers, the coordination around the copper centers in **4** is distorted square-pyramidal (Figure 4). The steric crowding around the copper centers, owing to the four phenyl substituents of azophenine, likely prevents the coordination of the third pyridine arm of the tmpa ligand. The two nitrogen donors from azophenine, together with an amine and a pyridine nitrogen donor atom from tmpa, form a nearly square-planar environment around each copper center. The distances between the copper centers and these four donor atoms are relatively short (between 1.97 and 2.05 Å, Table 2). Additionally, there is a fifth donor atom that is the second pyridine arm of tmpa. The Cu−N distance in that case is 2.370(2) Å that is significantly longer than the four former distances mentioned above. Thus, the coordination environment around the copper centers can be described as 4 + 1 distorted square-pyramidal. Also, the metal−ligand bond distances within the plane of the bridging ligand indicate that the magnetic orbitals $d_{x_2-y_2}$ of the copper centers lie in the plane containing the donor atoms of the bridging ligand.[3]

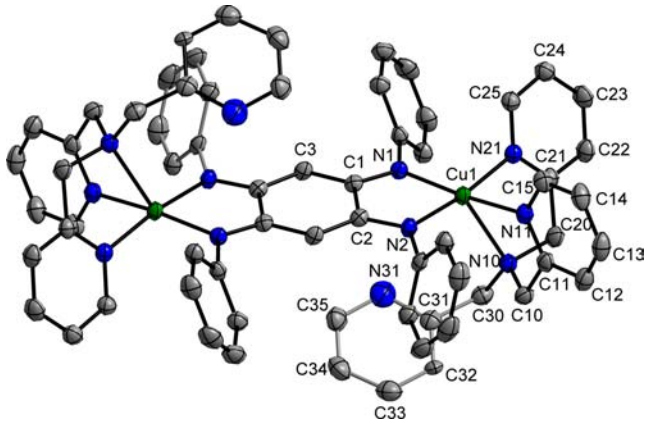

Figure 4. ORTEP plot of **4**. Ellipsoids are drawn at 50% probability. Hydrogen atoms and counteranions have been omitted for clarity.

All the C−N bond distances within the bridging ligand in **4** are virtually identical in length (Table 3). Also, the C1−C3 and C2−C3 distances are nearly identical. In contrast, the C1−C2 distance is 1.499(3) Å and is in the range expected for a single bond. Thus, the bridging ligand in **4** exhibits complete delocalization of its double bonds, and this is best described as a delocalized $6\pi + 6\pi$ system that is connected by single bonds (Scheme 3). Such a merocyanine type of bonding has been previously observed with other dinuclear complexes of azophenine and related ligands.[12b,d,e]

From the discussion of bond lengths within the bridging ligands in the coordinated form in **1**−**4**, it is seen that localization of double bonds in **1**−**3** is observed, leading to the preference for a *p*-quinonoid type of structure (Scheme 3). In contrast, a "bis-allyl" kind of structure is preferred in **4** (Scheme 3) that leads to a complete delocalization of the double bonds. A possible explanation for this phenomenon is the larger electronegativity difference between C and O (as compared to C and N), which leads to the preferential localization of the negative charges on the more electronegative O atoms in **1**−**3** and hence to the stabilization of the *p*-quinonoid form. For **4**, which has an all nitrogen donor containing bridging ligand, the electronegativity difference between C and N is smaller, and this probably leads to enhanced delocalization of the negative charge leading to a "bis-allyl" electronic structure.

The intramolecular Cu−Cu distances for the complexes **1**, **2**, **3**, and **4** are 8.285(2), 8.016(2), 7.766(2), and 7.834 Å, respectively. The rather pronounced difference in metal−metal distances between **1**, **2** and **3**, **4** reflects again the different orientation of the Jahn−Teller axis in these molecules.

Cyclic Voltammetry, Magnetism, and DFT Calculations. Cyclic voltammetry of complexes **1**−**4** was investigated in CH_3CN/0.1 M Bu_4NPF_6 to determine their redox potentials. Complex **1**, which contains the "most electronegative" bridge displayed two one-electron reversible reduction steps at −0.44 and −0.92 V (Figure S1, Supporting Information). In contrast, **2** displayed only one one-electron reversible step at −0.63 V, with the second reduction step probably lying outside the solvent window (Figure S2, Supporting Information). The replacement of the more electronegative Cl in **1** with H in **2** leads to a shift of the reduction potentials to higher negative values. Both **1** and **2** also display an irreversible oxidation step, the potential of which is similar for both complexes. For **3** and **4**, it was not possible to identify any defined redox processes. These complexes likely undergo large reorganizations, and possible decompositions

dx.doi.org/10.1021/ic400955c | *Inorg. Chem.* 2013, 52, 10332−10339

following redox processes, making all waves in cyclic voltammetric experiments ill-defined and irreversible.

The magnetic properties of complexes **1**−**4** were investigated with SQUID susceptometry. Effective magnetic moments, μ_{eff}, measured on a microcrystalline sample of **1**−**4** are in the range of 2.5−2.7 μ_B at room temperature (Figure 5). These values point

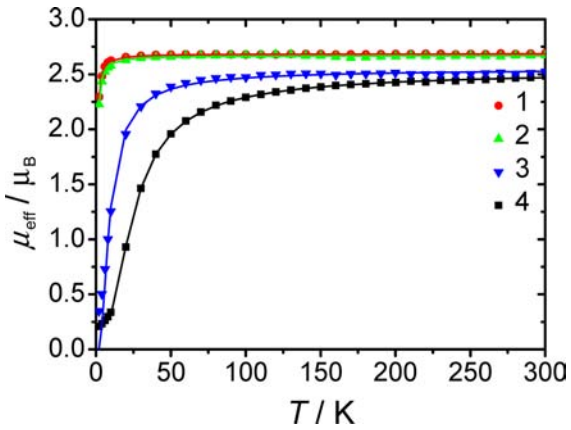

Figure 5. Temperature-dependent effective magnetic moment measured on microcrystalline **1**−**4** at an external field of 1 T; the solid lines are the best fits obtained with the following parameters: (a) **1**, $g = 2.19$, $J = -0.63$ cm^{-1}; (b) **2**, $g = 2.18$, $J = -0.73$ cm^{-1}; (c) **3**, $g = 2.09$, $J = -8.8$ cm^{-1}; (d) **4**, $g = 2.09$, $J = -23.2$ cm^{-1}, 2.1% of paramagnetic impurity, $S = 1/2$.

to the presence of two essentially magnetically uncoupled Cu(II) ions ($S_{Cu1} = S_{Cu2} = 1/2$) at room temperature. The effective magnetic moment, $\mu_{eff} = (\mu_1^2 + \mu_2^2)^{1/2} = (3 + 3)^{1/2} = 2.45\ \mu_B$, is expected for two noninteracting $S = 1/2$ paramagnetic centers without spin−orbit coupling (spin-only approximation). The effective magnetic moments for **1** and **2** remain nearly constant in the temperature range of 30−300 K; at lower temperatures, μ_{eff} gradually decreases, reaching the values 2.30 and 2.23 μ_B at 2 K for **1** and **2**, respectively. Such a decrease of μ_{eff} at low temperatures indicates a weak antiferromagnetic coupling between two Cu(II) ions in **1** and **2**. The effective magnetic moments for **3** and **4** start to decrease at higher temperatures and reach much lower values at 2 K (0.35 and 0.21 μ_B, respectively) compared to **1** and **2**. These provide evidence for a *stronger* antiferromagnetic coupling between the two Cu(II) ions in **3** and **4** than those in **1** and **2**.

To quantify magnetic coupling, temperature-dependent magnetic susceptibility data for **1**−**4** were fitted using a spin-Hamiltonian

$$\hat{\mathbf{H}} = \mu_B g_1 \hat{\mathbf{S}}_1 \mathbf{B} + \mu_B g_2 \hat{\mathbf{S}}_2 \mathbf{B} - 2J \hat{\mathbf{S}}_1 \hat{\mathbf{S}}_2 \quad (1)$$

where the first two terms represent an electron Zeeman effect for each Cu(II) ion and the third term accounts for intramolecular interactions between paramagnetic ions with isotropic exchange coupling constant J. The g values for two copper-based paramagnets are assumed to be equal: $g_1 = g_2 = g$.

The best fit parameters are $g = 2.19$, $J = -0.63$ cm^{-1} for **1**, and $g = 2.18$, $J = -0.73$ cm^{-1} for **2** (Figure 5, χ^{-1} vs T and χ vs T representations are given in the Supporting Information). Thus, the intramolecular spin−spin coupling between the two copper(II) ions is very similar and very small for **1** and **2**. In contrast to **1** and **2**, complexes **3** and **4** reveal much stronger intramolecular coupling between the two metal ions: the best fits provide $J = -8.8$ cm^{-1} and $J = -23.2$ cm^{-1} for **3** and **4**, respectively (Figure 5).

We assume that there are two reasons for the increase in the J values on moving from **1** and **2** to **3** and **4**. One reason is the rise in energy of the HOMO of the bridging ligand on moving from L^1_{-2H} to L^4_{-2H} that will bring the orbitals of the bridging ligand energetically closer to the copper-based magnetic orbitals. This increase in energy can be explained by the substitution of the more electronegative "Cl" with less electronegative "H" in the bridge on moving from L^1_{-2H} to L^2_{-2H}. However, as can be seen from the J values obtained for **1** and **2**, the effect of this substitution on the exchange coupling is marginal. The energy of the HOMO would also increase on making an [O] for [NR] isoelectronic substitution on the bridging ligand, and such a substitution should affect the exchange coupling more drastically because the heteroatom donors make a large contribution to the HOMO of the bridging ligands. Accordingly, the exchange coupling is seen to be much stronger for **3** and **4**. However, there is also a second effect that needs to be considered for the complexes discussed here. The coordination geometry around the Cu(II) ions is also drastically changed on moving from **1** and **2** to **3** and **4**. As has been stated during the discussion of structural data, for both **1** and **2**, the longer axis of the octahedron lies in the plane where the Cu(II) centers interact with the bridging ligand. The effect of this is the moving of the important copper-based magnetic orbitals $d_{x_2-y_2}$ away from the plane where the copper centers overlap with the donor atoms of the bridging ligand. Thus, for **1** and **2**, the magnetic orbitals of the Cu(II) centers are oriented in a unfavorable way to interact with the bridging ligand. For **3**, the long axis of the octahedron around the Cu(II) center is perpendicular to the plane containing the Cu(II) center and the donor atoms of the bridging ligand. This means that the magnetic orbitals $d_{x_2-y_2}$ can now orient more toward the plane of interaction with the bridge, and this leads to a favorable exchange interaction and a larger J value. The best case is for **4**, where, because of steric constraints, the Cu(II) centers are just 4 + 1 coordinated. Thus, the plane containing the Cu(II) center and the donor atoms of the bridge have strong bonds, and the axial ligand makes only a weak bond to the copper centers. Such an orientation is ideal for the $d_{x_2-y_2}$ magnetic orbitals to be appropriately placed for interaction with the bridge and results in the strongest coupling in the series.

DFT calculations were carried out to gain insights into the spin density distribution in the complexes, with a particular focus on the coordinating heteroatoms of the bridging ligands and to look at the orientation of the frontier orbitals. Additionally, this method was also used to calculate exchange coupling constants. Geometry optimizations (with the BP86 functional) reproduced the structural parameters with reasonable accuracy, with a good match obtained with the experimentally observed trends in bond lengths. For example, the longest copper−ligand distance observed experimentally in **4** is 3.781 Å for the Cu1−N31 bond. DFT calculations also show this bond to be the longest in **4** with a distance of 3.521 Å (Table S1, Supporting Information). The orientation of the longest axis around the Cu(II) centers (Jahn−Teller axis), as discussed in the experimental X-ray structural section above, is also accurately reproduced by DFT calculations. Hence, for **1**, the Cu1−O2 (expt. 2.550 Å) and the Cu1−N11 (expt. 2.257 Å) bonds make up the longest axis around the Cu(II) centers. DFT calculations on **1** deliver Cu1−O2 and Cu1−N11 distances of 2.374 and 2.293 Å, respectively, and sets the O2−Cu1−N11 as the longest axis around that

dx.doi.org/10.1021/ic400955c | *Inorg. Chem.* 2013, 52, 10332−10339

Cu(II) center (Table S1). These structural trends on metal−ligand bond distances are reproduced for all the four complexes by DFT calculations. The trends in bond distances within the bridging ligands are also accurately reproduced by DFT calculations. Thus, the C1−C2 bond is the longest experimentally observed bond within the bridging ligands in all the complexes. DFT calculations also show C1−C2 to be the longest bond (e.g., for **1**, expt. 1.538 Å, calculated 1.551 Å). The localization vs delocalization of bonds within the bridges is also nicely reproduced by DFT calculations. For example, the experimental bond lengths for C1−C3 and C2−C3 in **2** are 1.389 and 1.410 Å, respectively, displaying bond localization. DFT calculations deliver values of 1.401 and 1.422 Å, respectively, for those bonds, and confirm bond localization. In contrast, for **4**, the experimental C1−C3 and C2−C3 bond distances are 1.392 and 1.395 Å, respectively, showing bond delocalization. DFT calculations produce values of 1.414 and 1.411 Å, respectively, for those bonds, confirming bond delocalization within the bridge in **4**. (Table S1). Following geometry optimization of the X-ray coordinates, several functionals were used for calculating the *J* values for the complexes by employing the broken symmetry (BS) approach (Table 4).

Table 4. DFT Calculated *J* Values [cm^{-1}][a]

	1	2	3	4
expt.	−0.63	−0.73	−8.80	−23.2
B2PLYP	−0.11	−0.54	−15.0	−22.8
B3LYP	−2.03	−3.55	−30.5	−50.7
BP86	−14.1	−26.5	−104	−158

[a]In DFT, *J* is defined as $J = E(BS) - E(HS)$.

All the three functionals used could correctly reproduce the experimental trends in the *J* values (**4** > **3** > **2** > **1**). However, the BP86 functional was found to dramatically overestimate the absolute *J* values for all complexes. Calculations using the hybrid functional B3LYP reproduced the experimental values of **1** and **2** much better, but still overestimated the values of **3** and **4**. Therefore, the perturbatively corrected B2PLYP functional was tested, which delivered absolute *J* values with high accuracy and also confirmed the antiferromagnetic coupling between the spin centers.

Figure S7 (Supporting Information) shows the magnetic orbitals of **1**−**4**, which were obtained from the BS calculations. It is clearly seen that the orientation of the magnetic orbitals in **1** and **2** differs from that in **3** and **4**. In **1** and **2**, the magnetic orbitals are perpendicular to the plane of the bridging ligand. In contrast, the magnetic orbitals of **3** and **4** are within the plane of the bridging ligand. Thereby, the calculations nicely confirm the assumptions based on the bond length analysis of the molecular structures (vide supra). Furthermore, the orbital picture explains the fact that substitution at the 3- and 6-position of the quinone ligand has only a marginal effect on the exchange coupling. This is because these substituents do not contribute to the magnetic orbitals, as can be seen in **1** and **2**.

Figure 6 shows the calculated spin densities of the BS calculations, and relevant values are given in Table 5. Again, the spin densities in **1** and **2** are perpendicular to the bridging ligand. Hence, the total spin density is only delocalized over one of the coordinating O atoms from the bridging ligands through covalent interactions, whereas the other O atom has only negligible spin density. This is in line with the different Cu−O

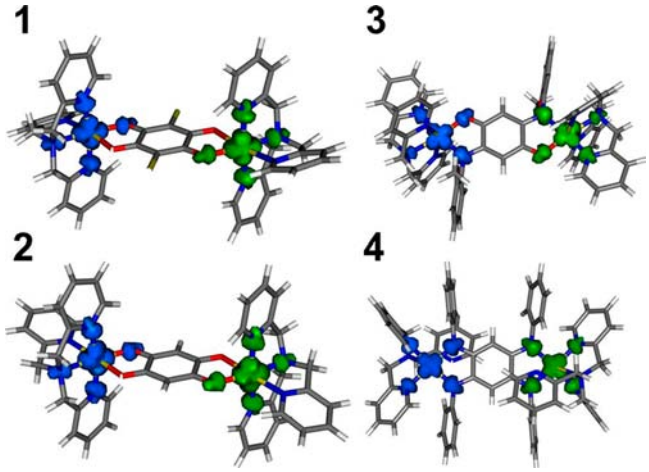

Figure 6. Calculated spin densities obtained from BS calculations with the B2PLYP functional (blue represents positive, whereas green stands for negative spin densities).

Table 5. Löwdin Spin Populations in Complexes 1−4 Calculated with the B2PLYP Functional (Only the Copper Centers and the Donor Atoms of the Quinonoid Ligands Are Considered)

	1	2	3	4
Cu1	0.830	0.833	0.836	0.792
O1	0.037	0.037	0.051	
O2	0.005	0.006		
N1				0.081
N2			0.079	0.079
Cu2	−0.830	−0.833	−0.834	−0.792
O11	−0.037	−0.037	−0.053	
O22	−0.005	−0.006		
N11				−0.081
N22			−0.078	−0.079

distances, and the weak antiferromagnetic coupling observed for **1** and **2**. In contrast, the spin densities in **3** and **4** are located within the plane of the bridging ligand. In the complexes **3** and **4**, the spin densities are equally distributed over both coordinating heteroatoms. In **3**, the oxygen and nitrogen atoms of the quinone bridge carry ±5.1% and ±7.8% of the spin density, whereas, in **4**, the nitrogen atoms of the quinone ligand carry ±7.9% and ±8.1% of the total spin population. Hence, the total spin density located at the bridging ligand is distinctly higher in **4**. The high spin density at both coordinating donor atoms is responsible for the effective exchange coupling in **3** and **4**. Furthermore, the better polarizability of nitrogen compared to that of oxygen is responsible for the most efficient exchange coupling in **4**. Thus, the amount of spin density on the donor atoms of the bridge, as calculated by DFT methods, directly correlates with the magnitude of the exchange coupling, providing also a quantitative measure from the calculations.

The DFT calculations are seen to nicely reproduce the trends in the *J* values and also their absolute values. Additionally, these calculations uncover two different exchange mechanisms in **1** and **2** compared to **3** and **4**, which can be explained by the different orientation of the magnetic orbitals. Not only is the effective exchange coupling in **3** and **4** related to the pathway of spin exchange but also the higher spin density at the nitrogen donor atoms compared to the oxygen donor atoms further facilitates the spin−spin interaction, as confirmed experimentally.

dx.doi.org/10.1021/ic400955c | *Inorg. Chem.* 2013, 52, 10332−10339

CONCLUSIONS

Summarizing, we have presented here the synthesis and structural characterization of four related dicopper(II) complexes with the same coligands and bridging quinone ligands that contain either an [O,O,O,O], [O,N,O,N], or a [N,N,N,N] donor set. In **1**−**3**, the Cu(II) centers are present in a Jahn−Teller distorted octahedral coordination environment. Despite these similarities, for **1** and **2**, the elongated axis of the octahedron lies in the plane of the bridging ligand, whereas, for **3**, this axis is perpendicular to the aforementioned plane. In **4**, the Cu(II) centers are in a distorted square-pyramidal environment. The bridging quinones in **1**−**3** display a *p*-quinonoid type structure with localized double bonds. In contrast, in **4**, the bridging ligand shows delocalization of double bonds, and formation of a "bis-allyl" type of bridge. The fits for temperature-dependent magnetic susceptibility data for **1**−**4** reveal a strong dependence of the exchange coupling constant (J) on the nature of the bridge. Both the increase in the HOMO energies of the bridge on moving from **1** to **4** as well as the different coordination geometry enforced by the bridging ligands on the Cu(II) centers have been invoked to explain the differences in exchange coupling constants. DFT calculations have been used to corroborate the experimental trend in exchange coupling and to also show the increase in spin density on the coordinating heteroatoms on making an [O] for [NR] substitution on the bridging quinone ligands. Furthermore, DFT calculations revealed two different exchange pathways in **1** and **2** compared to **3** and **4**, which is due to the different orientation of the respective magnetic orbitals. To the best of our knowledge, this is the first time that such a systematic study has been carried out on quinone-bridged dicopper(II) complexes where the copper center can potentially have six donating ligands. Our results show the influence on the coordinating geometry and spin−spin coupling that can be induced by a systematic variation of the quinone bridges. This is also one of the rare occasions where an [O,N,O,N] as well as a [N,N,N,N] donor containing quinone bridge has been combined with paramagnetic 3d metal centers for investigating bridge-mediated spin−spin coupling. In view of the large differences in spin−spin coupling that can be induced by incorporating such hitherto unused bridging ligands, it will be intriguing to use these [NR] containing bridges in combination with other 3d metal centers for investigating magnetic phenomena. Our future work will focus in that direction.

EXPERIMENTAL SECTION

Materials and General Methods. All chemicals were used as received unless otherwise mentioned. The ligands L^3 and L^4 were synthesized according to reported procedures.[7f,g,11] Elemental analyses were performed with a PerkinElmer Analyzer 240. Cyclic voltammetry was carried out in 0.1 M Bu_4NPF_6 solution using a three-electrode configuration (glassy carbon working electrode, Pt counter electrode, Ag wire as pseudoreference) and a PAR 273 potentiostat and function generator. The ferrocene/ferrocenium (Fc/Fc^+) couple served as internal reference.

Magnetic Measurements. Magnetic susceptibility measurements were performed on microcrystalline samples with an MPMS XL SQUID magnetometer (Quantum Design) at an external field of 1 T (=10 kOe) and variable temperature (2−300 K). The obtained data were corrected for the underlying diamagnetism. The experimental data were fitted using the spin-Hamiltonian shown in eq 1.

DFT Calculations. The program package ORCA 2.8 was used for all calculations.[14] Coordinates of the crystal structures were used as starting points for the geometry optimization by the spin-unrestricted DFT method with the BP86 functional.[15] Criteria for the geometry optimization were set to default values (OPT), and "tight" convergence criteria were used for SCF calculations (TIGHTSCF). The triple-ζ basis sets with one-set of polarization functions[16] (TZVP) were used for transition metal and nitrogen atoms, and the double-ζ basis sets with one set of polarization functions[17] (SVP) were used for all other atoms. Single-point calculations were performed with the BP86,[15] B3LYP,[18] and B2PLYP[19] functionals. The resolution of the identity approximation (RIJCOSX) was employed[20,21] with matching auxiliary basis sets.[21] All spin densities were calculated according to Löwdin population analysis[22] and were visualized via the program Molekel.[23] The magnetic coupling was investigated by the broken symmetry approach.[24]

Synthesis. ***1***. tmpa·3$HClO_4$ (160 mg, 0.27 mmol) and $Cu(ClO_4)_2$·$6H_2O$ (100 mg, 0.27 mmol) were dissolved in MeOH (20 mL). NEt_3 (0.3 mL) was added, and the solution was stirred for 30 min. Meanwhile, chloranilic acid (29 mg, 0.14 mmol) was dissolved in MeOH (10 mL) and deprotonated with NEt_3 (0.1 mL). The solution of the deprotonated ligand was added dropwise to the metal precursor solution and stirred for 5 min. The reaction was kept untouched overnight, and the next day, single crystals suitable for X-ray diffraction could be filtered off. The product could be isolated as blue crystals in 65% yield (101 mg). Anal. Calcd for $C_{42}H_{36}Cl_4Cu_{28}O_{12}$: C, 45.30; H, 3.26; N, 10.06. Found C, 44.95; H, 3.27; N, 9.66.

2. tmpa·3$HClO_4$ (160 mg, 0.27 mmol) and $Cu(ClO_4)_2$·$6H_2O$ (100 mg, 0.27 mmol) were dissolved in MeOH (20 mL). NEt_3 (0.3 mL) was added, and the solution was stirred for 30 min. Meanwhile, 2,5-dihydroxybenzoquinone (20 mg, 0.14 mmol) was dissolved in MeOH (10 mL) and deprotonated with NEt_3 (0.1 mL). The solution of the deprotonated ligand was added dropwise to the metal precursor solution and stirred for 5 min. The reaction was kept untouched overnight, and the next day, single crystals suitable for X-ray diffraction could be filtered off. The product could be isolated as blue crystals in 60% yield (88 mg). Anal. Calcd for $C_{42}H_{38}Cl_2Cu_2N_8O_{12}$: C, 48.28; H, 3.67; N, 10.72. Found C, 47.40; H, 3.69; N, 10.25.

3. tmpa·3$HClO_4$ (160 mg, 0.27 mmol) and $Cu(ClO_4)_2$·$6H_2O$ (100 mg, 0.27 mmol) were dissolved in MeOH (20 mL). NEt_3 (0.3 mL) was added, and the solution was stirred for 30 min. Meanwhile, the ligand L^3_{-2H} (49 mg, 0.14 mmol) was dissolved in MeOH (10 mL) and deprotonated with NEt_3 (0.1 mL). The solution of the deprotonated ligand was added dropwise to the metal precursor solution, and the resulting solution was refluxed for 1 h. After cooling down, a brown precipitate could be filtered off. The product was obtained in 80% yield (141 mg). After salt metathesis with $NaBPh_4$, single crystals suitable for X-ray diffraction could be grown by slow diffusion of diethylether into an acetonitrile solution. Anal. Calcd for $C_{56}H_{52}Cl_2Cu_2N_{10}O_{12}$: C, 53.59; H, 4.18; N, 11.16. Found C, 53.14; H, 4.11; N, 10.62.

4. tmpa·3$HClO_4$ (474 mg, 0.80 mmol) and $Cu(ClO_4)_2$·$6H_2O$ (296 mg, 0.80 mmol) were dissolved in MeOH (20 mL) under a nitrogen atmosphere. *N*,*N*-diisopropylethylamine (0.3 mL) was added, and the solution was stirred for 30 min. Diethylether (30 mL) was added to precipitate the product, which was dried at high vacuum to remove traces of water. Azophenine (154 mg, 0.35 mmol) was dissolved in DCM (20 mL) and deprotonated overnight with *N*,*N*-diisopropylethylamine (0.3 mL). The solution was then added to the copper precursor, and after addition of toluene (30 mL), the solution was refluxed for 8 h. Next, a dark solid could be isolated by filtration. The solid was thoroughly washed with THF to remove unreacted azophenine. Recrystallization from CH_3CN/CH_2Cl_2 and Et_2O was repeated several times. Block-shaped dark crystals (20 mg) could be isolated in very low yields (2%), which were suitable for X-ray diffraction. Anal. Calcd for $C_{66}H_{58}Cl_2Cu_2N_{12}O_8$·$0.5CH_2Cl_2$: C, 57.56; H, 4.29; N, 12.11. Found C, 57.81; H, 4.41; N, 12.19.

X-ray Crystallography. Suitable single crystal of **1**−**4** were selected and mounted onto a thin glass fiber. X-ray intensity data were measured at 150 K on an Oxford Gemini S Ultra diffractometer with the Enhance X-ray Source of Cu Kα radiation (λ = 1.54178 Å) using the ω−φ scan technique[25] or with a four circle diffractometer P4 (Siemens, Madison (USA)) at 173 K. Empirical absorption correction was applied using spherical harmonics implemented in the SCALE3 ABSPACK scaling algorithm.[26] The structure was solved by direct methods and refined by full-matrix least-squares against F^2 of all data using the SHELXTL

program package.[27] Anisotropical thermal factors were assigned to the non-hydrogen atoms, while the positions of the hydrogen atoms were generated geometrically, assigned isotropic thermal parameters, and allowed to ride on their respective parent atoms before the final cycle of least-squares refinement. CCDC 911118−911121 contains the supplementary crystallographic data for this paper. These data can be obtained free of charge from the Cambridge Crystallographic Data Centre via www.ccdc.cam.uk/data_request.cif.

■ ASSOCIATED CONTENT

Ⓢ Supporting Information

Figures showing cyclic voltammograms, temperature-dependent magnetic susceptibility data, and magnetic orbitals; tables containing selected metal−ligand bond lengths, intraligand bond lengths, and selected angles; and optimized structure data for **1**−**4**. This material is available free of charge via the Internet at http://pubs.acs.org.

■ AUTHOR INFORMATION

Corresponding Author

*E-mail: biprajit.sarkar@fu-berlin.de.

Notes

The authors declare no competing financial interest.

■ ACKNOWLEDGMENTS

We are indebted to the Fonds der Chemischen Industrie (FCI) for financial support of this project (Chemiefondsstipendium for D.S.). M.M.K. thanks the FCI for a Liebig Fellowship and the DFG for financial support. Prof. Karsten Meyer is acknowledged for providing access to the SQUID magnetometer. Corinna Schelzel is acknowledged for experimental help. We thank BWGrid for providing us with computer time.

■ DEDICATION

Dedicated to Prof. W. Uhl on the occasion of his 60th birthday.

■ REFERENCES

(1) (a) Gispert, J. R. *Coordination Chemistry*; Wiley-VCH Verlag GmbH & Co. KGaA: Weinheim, Germany, 2008. (b) Kahn, O. *Angew. Chem., Int. Ed.* **1985**, *24*, 834. (c) Kahn, O. *Molecular Magnetism*; VCH Publishers: New York, 1993. (d) Gatteschi, D.; Kahn, O.; Miller, J. S.; Palacio, F., Eds. *Magnetic Molecular Materials*; Kluwer Academic Publishers: Dordrecht, The Netherlands, 1991; Vol. *198*.

(2) (a) Kawata, S.; Kitagawa, S.; Kondo, M.; Furuchi, I.; Munakata, M. *Angew. Chem., Int. Ed.* **1994**, *33*, 1759. (b) Kuwahara, M.; Kabir, Md.; Yamada, K.; Adachi, K.; Kumagai, H.; Narumi, Y.; Kindo, K.; Kitagawa, S.; Kawata, S. *Inorg. Chem.* **2004**, *43*, 92. (c) Gallert, S.; Weyhermüller, T.; Wieghardt, K.; Chaudhuri, P. *Inorg. Chim. Acta* **1998**, *274*, 111. (d) Chaudhuri, P.; Oder, K. *J. Chem. Soc., Dalton Trans.* **1990**, 1597. (e) Verdaguer, M.; Michalowicz, A.; Girerd, J. J.; Alberding, N.; Kahn, O. *Inorg. Chem.* **1980**, *29*, 327. (f) Pierpont, C. G.; Francesconi, L. C.; Hendrickson, D. N. *Inorg. Chem.* **1977**, *16*, 2367.

(3) Kitagawa, S.; Kawata, S. *Coord. Chem. Rev.* **2002**, *224*, 11 and references therein.

(4) Tinti, F.; Verdaguer, M.; Kahn, O.; Savariault, J.-M. *Inorg. Chem.* **1987**, *26*, 2380.

(5) (a) Ward, M. D. *Inorg. Chem.* **1996**, *35*, 1712. (b) Leschke, M.; Melter, M.; Lang, H. *Inorg. Chim. Acta* **2003**, *350*, 114. (c) Carbonera, C.; Dei, A.; Letard, J.-F.; Sangregorio, C.; Sorace, L. *Angew. Chem., Int. Ed.* **2004**, *43*, 3136. (d) Miller, J. S.; Min, K. S. *Angew. Chem., Int. Ed.* **2009**, *48*, 262. (e) Therrien, B.; Süss-Fink, G.; Govindaswamy, P.; Renfrew, A. K.; Dyson, P. J. *Angew. Chem.* **2008**, *120*, 3833.

(6) Schweinfurth, D.; Weisser, F.; Sarkar, B. *Nachr. Chem.* **2009**, *57*, 862.

(7) (a) Kumbhakar, D.; Sarkar, B.; Maji, S.; Mobin, S. M.; Fiedler, J.; Aparicio, R. J.; Kaim, W.; Lahiri, G. K. *J. Am. Chem. Soc.* **2008**, *130*, 17575. (b) Keyer, T. E.; Forster, R. J.; Jayaweera, P. M.; Coates, C. G.; McGarvey, J. J.; Vos, J. G. *Inorg. Chem.* **1998**, *37*, 5925. (c) Kar, S.; Sarkar, B.; Ghumaan, S.; Janardanan, D.; van Slageren, J.; Fiedler, J.; Puranik, V. G.; Sunoj, R. B.; Kaim, W.; Lahiri, G. K. *Chem.—Eur. J.* **2005**, *11*, 4901. (d) Masui, H.; Freda, A. L.; Zerner, M. C.; Lever, A. B. P. *Inorg. Chem.* **2000**, *39*, 141. (e) Weisser, F.; Huebner, R.; Schweinfurth, D.; Sarkar, B. *Chem.—Eur. J.* **2011**, *17*, 5727. (f) Das, H. S.; Weisser, F.; Schweinfurth, D.; Su, C.-Y.; Bogani, L.; Fiedler, J.; Sarkar, B. *Chem.—Eur. J.* **2010**, *16*, 2977. (g) Schweinfurth, D.; Das, H. S.; Weisser, F.; Bubrin, D.; Sarkar, B. *Inorg. Chem.* **2011**, *50*, 1150.

(8) Margraf, G.; Kretz, T.; de Biani, F. F.; Lasi, F.; Loschi, S.; Zanello, P.; Bats, J. W.; Wolf, J.; Removic-Langer, K.; Lang, M.; Prokofiev, A.; Assmus, W.; Lerner, H.-W.; Wagner, M. *Inorg. Chem.* **2006**, *45*, 1277.

(9) (a) Zhang, D.; Jin, G.-X. *Organometallics* **2003**, *22*, 2851. (b) Scheuermann, S.; Kretz, T.; Vitze, H.; Bats, J. W.; Bolte, M.; Lerner, H.-W.; Wagner, M. *Chem.—Eur. J.* **2008**, *14*, 2590.

(10) Jia, W.-G.; Han, Y.-F.; Lin, Y.-J.; Weng, L.-H.; Jin, G.-X. *Organometallics* **2009**, *28*, 3459.

(11) (a) Kimisch, C. *Ber. Dtsch. Chem. Ges.* **1875**, *8*, 1026. (b) Ruggli, P.; Buchmeier, F. *Helv. Chim. Acta* **1945**, *28*, 850.

(12) (a) Rall, J.; Stange, A. F.; Hübler, K.; Kaim, W. *Angew. Chem., Int. Ed.* **1998**, *37*, 2681. (b) Siri, O.; Taquet, J.-P.; Collin, J.-P.; Rohmer, M.-M.; Bénard, M.; Braunstein, P. *Chem.—Eur. J.* **2005**, *11*, 7247. (c) Su, Y.; Zhao, Y.; Gao, J.; Dong, Q.; Wu, B.; Yang, X.-Y. *Inorg. Chem.* **2012**, *51*, 5889. (d) Siri, O.; Braunstein, P.; Taquet, J.-P.; Collin, J.-P.; Welter, R. *Dalton Trans.* **2007**, 1481. (e) Siri, O.; Braunstein, P.; Rohmer, M.-M.; Bénard, M.; Welter, R. *J. Am. Chem. Soc.* **2003**, *125*, 13793.

(13) (a) Shearer, J.; Zhang, C. X.; Zakharov, L. N.; Rheingold, A. L.; Karlin, K. D. *J. Am. Chem. Soc.* **2005**, *127*, 5469. (b) Miyazaki, S.; Ohkubo, K.; Kojima, T.; Fukuzumi, S. *Angew. Chem., Int. Ed.* **2007**, *46*, 905. (c) Hirai, Y.; Kojima, T.; Mizutani, Y.; Shiota, Y.; Yoshizawa, K.; Fukuzumi, S. *J. Am. Chem. Soc.* **2008**, *47*, 5772. (d) Miyazaki, S.; Kojima, T.; Mayer, J. M.; Fukuzumi, S. *J. Am. Chem. Soc.* **2009**, *131*, 11615.

(14) Neese, F. *ORCA: An Ab Initio, Density Functional and Semiempirical Program Package*, version 2.8; Institut für Physikalische und Theoretische Chemie, Universität Bonn: Bonn, Germany, February 2011.

(15) Becke, A. D. *J. Chem. Phys.* **1993**, *98*, 5648.

(16) Schafer, A.; Huber, C.; Ahlrichs, R. *J. Chem. Phys.* **1994**, *100*, 5829.

(17) Schafer, A.; Horn, H.; Ahlrichs, R. *J. Chem. Phys.* **1992**, *97*, 2571.

(18) Lee, C. T.; Yang, W. T.; Parr, R. G. *Phys. Rev. B* **1988**, *37*, 785.

(19) Grimme, S. *J. Chem. Phys.* **2006**, *124*, 034108.

(20) (a) Baerends, E. J.; Ellis, D. E.; Ros, P. *Chem. Phys.* **1973**, *2*, 41. (b) Dunlap, B. I.; Connolly, J. W. D.; Sabin, J. R. *J. Chem. Phys.* **1979**, *71*, 3396. (c) Vahtras, O.; Almlof, J.; Feyereisen, M. W. *Chem. Phys. Lett.* **1993**, *213*, 514.

(21) (a) Eichkorn, K.; Treutler, O.; Ohm, H.; Haser, M.; Ahlrichs, R. *Chem. Phys. Lett.* **1995**, *242*, 652. (b) Eichkorn, K.; Weigend, F.; Treutler, O.; Ahlrichs, R. *Theor. Chem. Acc.* **1997**, *97*, 119.

(22) (a) Löwdin, P. O. *J. Chem. Phys.* **1950**, *18*, 365. (b) Löwdin, P. O. *Adv. Quantum Chem.* **1970**, *5*, 185.

(23) Portmann, S. *Molekel*, version 5.4.0.8; CSCS/UNI Geneva: Geneva, Switzerland, 2009.

(24) (a) Noodleman, L.; Davidson, E. R. *Chem. Phys.* **1986**, *109*, 131. (b) Noodleman, L. *J. Chem. Phys.* **1981**, *74*, 5737.

(25) *CrysAlis CCD*, Version 1.171.31.7.; Oxford Diffraction Ltd.: Abingdon, U.K., 2006.

(26) *CrysAlis RED*, Version 1.171.31.7; Oxford Diffraction Ltd.: Abingdon, U.K., 2006.

(27) *SHELXTL*, version 5. 10; Bruker Analytical X-ray Systems: Madison, WI, 1998.